Nanoscale

Accepted Manuscript

This article can be cited before page numbers have been issued, to do this please use: C. Ma, Z. Zhu, H. Wang, X. Huang, X. Zhang, X. Qi, H. Zhang, Y. Zhu, X. Deng, Y. Peng, Y. Han and H. Zhang, *Nanoscale*, 2015, DOI: 10.1039/C5NR01757B.

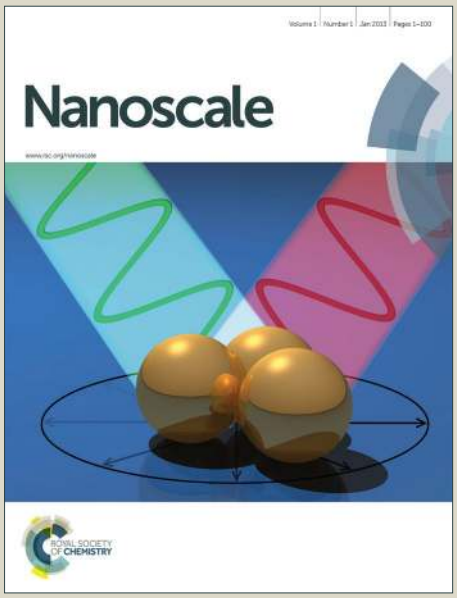

ROYAL SOCIETY OF CHEMISTRY

www.rsc.org/nanoscale

View Article Online
DOI: 10.1039/C5NR01757B

Nanoscale

RSCPublishing

ARTICLE

A General Solid-State Synthesis of Chemically-Doped Fluorescent Graphene Quantum Dots for Bioimaging and Optoelectronic Applications

Cite this: DOI: 10.1039/x0xx00000x

Received 00th February 2015,
Accepted 00th February 2015

DOI: 10.1039/x0xx00000x

www.rsc.org/

Chong-Bo Ma,[a] Zhen-Tong Zhu,[a] Hang-Xing Wang,[a] Xiao Huang,[b] Xiao Zhang,[b] Xiaoying Qi,[c] Hao-Li Zhang,[a,*] Yihan Zhu,[d] Xia Deng,[e] Yong Peng,[e] Yu Han[d] and Hua Zhang[b, *]

Graphene quantum dots (GQDs) have attracted increasing interest because of their excellent properties such as strong photoluminescence, excellent biocompatibility and low cost. Herein, we develop a general method for the synthesis of doped and undoped GQDs, which relies on direct carbonization of organic precursors at solid state.

Introduction

Graphene quantum dots (GQDs) have attracted great attention recently owning to their unique optical properties and promising applications in photovoltaics,[1] bioimaging[2] and drug delivery.[3] In the past few years, great efforts have been made to the synthesis of GQDs. However, the majority of the reported synthetic methods were mainly based on the top-down strategies with graphite,[4] graphite oxide[5] or even coal[6] as bulk starting materials.

Compared to the pristine GQDs, chemically doped carbon nanomaterials showed some attractive properties,[7] such as tunable electronic structure,[7a,b] visible-light photocatalytic activity,[7c] and negative differential resistance behaviour.[7d] Until now, several methods, including electrochemical,[8] hydrothermal,[9] solvothermal,[10] and organic synthesis methods,[11] have been used for preparation of chemically doped GQDs. In particular, the bottom-up methods, typically via the pyrolysis of small molecules under hydrothermal conditions, were successfully used to synthesize doped GQDs[9] and carbon nanodots.[12] The bottom-up approach showed advantages of low cost and precise control over synthetic conditions. However, most of the reported methods are only suitable for very few specific starting materials or precursors.[13] To date, there is still lack of general synthetic methods which can use a wide range of precursors to synthesize GQDs.

In this article, we report a general method for synthesis of various chemically doped GQDs from a wide range of precursors. This method is based on the direct carbonization of organic precursors at solid state under controlled experimental conditions. Depending on the chemical compositions of the different precursors, GQDs doped by different heteroatoms, including O, N, S and P, were successfully synthesized. Importantly, our method offers several advantages, such as easy operation, solvent free, wide precursor tolerance, short reaction time, low cost and scalable production.

Experimental details

Chemicals and materials

The organic precursors including ethylene diamine tetraacetic acid (EDTA), glucose, tartaric acid, sucrose, lysine, arginine, cysteine, cystine, dithiothreitol (DTT) and adenosine 5'-triphosphate disodium salt (ATP) were purchased from Sigma (St. Louis, MO, USA) and used as received. Ultrapure Milli-Q water (Milli-Q System, Millipore, Billerica, MA, USA) was used in all experiments.

Synthesis

The synthesis of GQDs from EDTA is described herein as an example. 0.5 g EDTA was loaded into a round bottom flask, and then heated in a sand bath at 260-280 ^{o}C with vigorous stirring. The white solid became dark brown in 5 min. After cooling down to room temperature, water was added to disperse the product. The undissolved residue was removed by centrifugation at 8,000 rpm for 5 min. The supernatant was further purified by centrifugation and filtration using AmiconUltra filter (Millipore, Billerica, MA) with a molecular mass cut-off of 10 kDa to remove large sheets. The final product was collected by dialyzing the aqueous solution with a dialysis membrane bag (MW 1000) for several days to fully remove the residual EDTA. The produced N and O doped GQD is referred to as E-GQD.

Under the similar reaction and purification conditions, GQDs from other precursors were also obtained, including glucose, sucrose, tartaric acid, arginine, lysine, ATP, cysteine, cystine and DTT. The optimal reaction temperatures are slightly different for each precursor, which has been described in the Supporting Information (SI).

Electrophoretic deposition

In order to show the effects of chemical doping, a plain GQD produced by citric acid (CA-GQDs)[13a] was also studied as a reference. Two indium tin oxide (ITO) electrodes (area of 1 × 1.1 cm^2) were used as anode and cathode, respectively. The electrodes

View Article Online
DOI: 10.1039/C5NR01757B Journal Name

were immersed in the aqueous dispersion of E-GQDs or CA-GQDs, with their distance kept at approximately 1.5 cm. A DC power source was used to provide the electric field controlled at 10 V/cm. After a deposition time ranging from 10-30 s, dark brown films were observed on the anode, and the electrodes were then dried in vaccum at 60 °C for 1 h prior to further characterization.

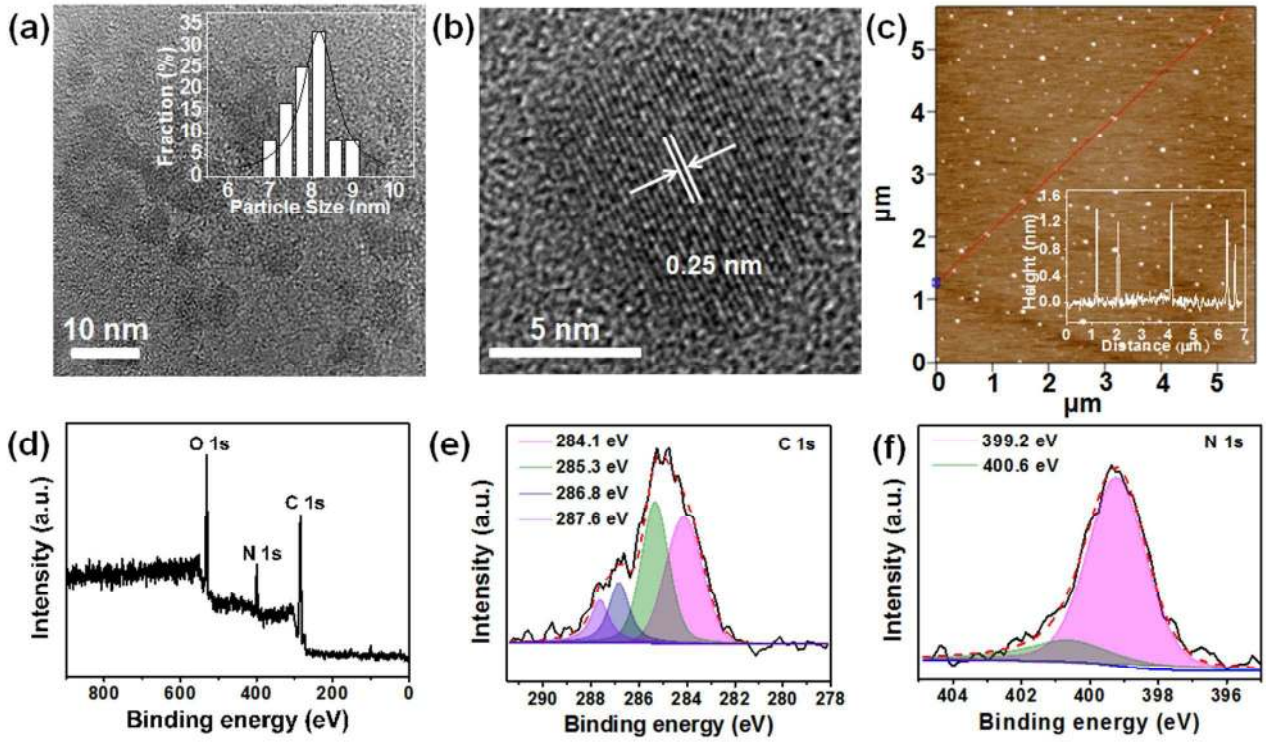

Figure 1. (a) TEM image of purified E-GQDs. Inset: Size distribution of E-GQDs with Gaussian fitting curve.The average size is 8.2 ± 1.2 nm. (b) HRTEM image of a typical E-GQD. (c) AFM image of E-GQDs. Inset: Height profile along the red line. (d) XPS survey spectrum and the deconvolution of C 1s spectrum (e) and N 1s spectrum (f) of E-GQDs.

Characterizations

The GQD solution was dropped onto a clean glass slide for X-ray diffraction (XRD) and Raman measurement, and onto a fresh silicon wafer for X-ray photoelectron spectroscopy (XPS) test and mica substrate for atomic force microscopy (AFM) observation. The transmission electron microscope (TEM) samples were prepared by dropping the ethanol suspension of GQDs onto a copper mesh. Certain amount of the powders of the precursors including EDTA, glucose, tartaric acid, sucrose, ATP, lysine, arginine, cysteine, cystine and DTT were used to do the thermo gravimetry analysis (TGA). Fourier transform infrared (FT-IR) samples were dried in vacuum from concentrated GQD aqueous solutions before tableting with KBr. XRD pattern was recorded by an X-ray diffract meter Bruker AXSD8 using Cu Kα radiation (40 kV, 200 mA) with a Ni filter. Raman spectrum was obtained by a confocal microscope Raman system (Renishaw in via Raman microscope). XPS spectra were collected on a multifunctional XPS/AES system (Kratos Axis Ultra DLD, Japan) by using Al Kα radiation (150 W, pass energy of 80 eV for survey spectrum, and 20 eV for high-resolution spectrum). TEM measurement was taken with TecnaiTMG2F30, operated at an accelerating voltage of 300 kV. Scanning electron microscopy (SEM, JSM-7600) was performed on a field emission SEM (FESEM) instrument (S-4800, Japan). AFM observation was carried out using an MFP3D microscope (Asylum Research, Goleta, CA, USA) with a silicon cantilever operating in tapping mode. TGA (model 1090; DuPont, Wilmington, DE) was conducted in a nitrogen flow from room temperature to 800 °C at a heating rate of 10 °C/min. The FT-IR spectra were obtained on a PerkinElmer Spectrum One Spectrometer (Shelton, CT, USA). The UV-vis absorption spectra were recorded using an UV-2450 spectrophotometer (Shimadzu, Japan). The fluorescence spectra were obtained from a FluoroMax-3 (Horiba Scientific) fluorometer. The fluorescence, dark-field and bright-field imaging experiments were operated on an Olympus IX51 inverted microscope with a Photometrics Cool SNAP-cf cooled CCD camera.

Cell culture and cytotoxicity assay

The RAW 264.7 (Mouse leukaemic monocyte macrophage cell line) cells were cultured in Dulbecco's modified eagle medium (DMEM) supplemented with 10% fetal bovine serum for 3 days in a humidified incubator at 37 °C in an atmosphere of 5% CO_2 prior to the imaging experiments. A standard cell counting Kit-8 (CCK-8) assay was used for the cytotoxicity assay. The microphage cells were seeded into 96-well plates at a density of 10,000 per well in 200 μL media and grew overnight. Then, the cells were incubated with various concentrations of E-GQDs (from 0 to 140 μg/mL) in phosphate buffered saline (PBS, pH 7.4) and the plate was incubated for 6 h in the incubator at 37 °C and 5% CO_2. Then, 10 μL of CCK-8 solution was added into each well of the plate, which was incubated for another 4 h at 37 °C and 5% CO_2. The absorbance of each sample at 450 nm was measured using a microplate reader (Bio-Rad, Hercules, CA, USA). The cell viability was calculated as the ratio of absorbance of sample well to that of control well (without E-GQDs).

Journal Name View Article Online DOI: 10.1039/C5NR01757B ARTICLE

The standard deviation of each measurement was calculated from three independent experiments.

Imaging E-GQD stained RAW 26 cells

The RAW 26 cells were seeded onto sterile cover-slips in the 8-well plate and allowed to adhere overnight at 37 ^{o}C and 5% CO_2. After removal of the medium by washing with PBS twice, the cells were incubated with 80 μg/mL of E-GQDs in PBS for 1 h at 37 ^{o}C and 5% CO_2. Subsequently, cells were washed three times with PBS to remove the unbound E-GQDs. To investigate the cellular uptake of E-GQDs, the RAW 264.7 cells were incubated with 80 μg/mL of E-GQDs in PBS (pH 7.4) for 1 h at 37 ^{o}C and 5% CO_2, then the cells were lysosome-stained with LysoTracker@Green for 10 min. Subsequently, cells were washed three times with PBS. Then the side of the coverslip with stained cells was topped by a glass slide, which was placed on the microscope to image the cells using the DAPI filter.

Photocurrent measurement

ITO glass coated with GQDs was used as working electrode. Pt was used as counter electrode. 0.05 M of Na_2S aqueous solution was used as electrolyte. The photocurrent responses were measured under pulsed light illumination with a 500 W Xe lamp as light source (100 mW/cm^2) at 10 s intervals of light-on and light-off at a constant potential of 0 V (vs. SCE).

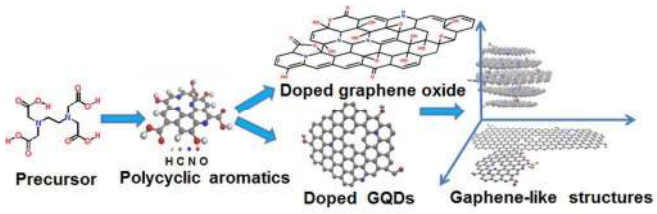

Figure 2. Schematic illustration of reaction process for preparation of E-GQDs and graphene-like structures from EDTA.

Results and discussion

As a typical example, the synthesis and characterization of nitrogen doped (N-doped) GQDs by using EDTA as precursor, referred to as E-GQDs, are demonstrated. In order to prepare E-GQDs, a glass flask containing the EDTA powder was immersed in a sand bath and heated to 260-280 ^{o}C under vigorous stirring for 5 min. The as-produced brown powder was dispersed in water, and then subjected to centrifugation at 8,000 r.p.m. for 5 min to remove the insoluble precipitate, followed by filtration using a tubular ultrafiltration membrane with molecular mass cut-off of 10 kDa. The final product was collected by dialyzing the aqueous solution with a dialysis membrane bag (MW 1000) for several days to fully remove the residual EDTA. In previous work, Chi has reported GQDs synthesis by direct carbonization of citric acid but only limited to confined precursor and no chemical doping was realized.[13a] To demonstrate the effects of chemical doping, we have also prepared the undoped GQDs from citric acid precursor, referred to as CA-GQD, and used it as reference.

The effect of reaction time and temperature on the yield of different types of nanostructures produced was studied systematically (Table S1, in SI). The corresponding products with different sizes are shown in Figure S1 in SI. Our experiments showed that the high-yield, uniform E-GQDs can only be obtained at a relatively short reaction time, typically a few minutes, with reaction temperature slightly above the decomposition temperature of the precursor. Specifically, the optimal experimental condition for synthesis of E-GQDs was found to be 5 min of reaction in the temperature range of 260-280 ^{o}C, which is slightly higher than the decomposition temperature of EDTA, i.e. 252 ^{o}C, measured by TGA (Figure S2, in SI). At lower reaction temperature, for example 240-260 ^{o}C, E-GQDs were synthesized in low yield (Table S1, in SI), while at higher reaction temperature (e.g. > 280 ^{o}C) or longer reaction time (e.g. 10 min), microsized flakes were produced (Figure S3, in SI). It is known that EDTA undergoes decarboxylation and produces various N-containing species at its decomposition temperature.[14] These species might gradually fuse together to give graphite-like structures under the solid-state reaction condition, which is supported by the fact that the N-containing compounds can be converted into various graphitic carbon nitride at much higher pyrolysis temperature (Figure 2).[15]

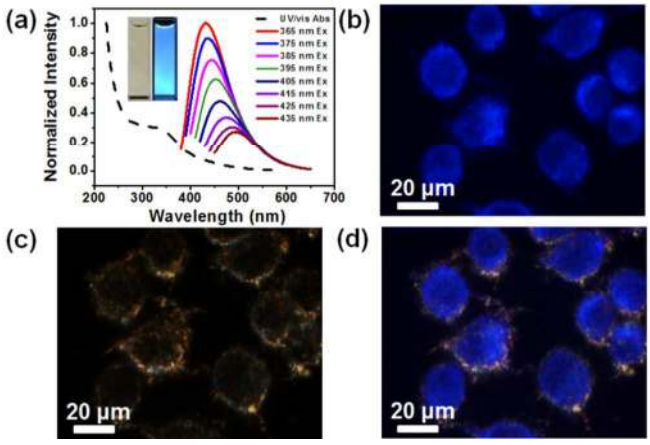

Figure 3. (a) Normalized UV/vis absorption (dash) and PL (solid) spectra of E-GQDs. Inset: Photographs of E-GQDs in aqueous solution under visible (left) and UV (right) light. (b) Fluorescence image of RAW 264.7 cells incubated with 80 μg/mL of E-GQDs. (c) The dark-field image corresponding to (b). (d) Overlay of (b) and (c).

The TEM data on the E-GQDs produced under the aforementioned optimized conditions suggest that the product contains mainly small particle-like nanostructures with size of 8.2 ± 1.2 nm (Figure 1a). From the high resolution TEM (HRTEM) images, the lattice spacing of 0.25 nm (Figure 1b), i.e. twice the spacing of (110) planes of graphite,[16a] and 0.21 nm (Figure S4, in SI), i.e. (100) lattice fringes of graphite,[16b] are observed. AFM measurement (Figure 1c) and the height distribution analysis (Figure S5a, in SI) suggest that the particle thicknesses is 1.5 ± 1.0 nm, narrower layer distribution than the reported 1-5 layers of N-doped GQDs produced by electrochemical method.[8] XPS spectra of E-GQDs show the predominant C 1s, O 1s and N 1s peaks (Figure 1d), which gives the atomic compositions of C, O and N at 44%, 42% and 14%, respectively. The N/C atomic ratio is 33%, much higher than that of reported N-GQDs (4.3%).[8] We have conducted a control experiment by synthesizing the E-GQDs under oxygen free condition. Table S2 in SI compares the compositions of the products prepared in the open air and the product in oxygen free atmosphere. The XPS data indicate that the product from the oxygen-free condition indeed has slightly higher carbon (49%) and lower oxygen content (36%), but the difference between the two products is not very significant. Because the precursors used in the synthesis are oxygen rich compounds, oxygen in air may participate in the reaction but does not change the composition significantly, and the oxygen content of the final products is mainly from the precursors. The deconvoluted C 1s peaks in Figure 1e consist of mainly four individual ones assignable to C–C (~284.1 eV),[17a] C–N (~285.3 eV),[8] C–O (~286.8 eV),[8] and C=O (~287.6 eV) bonds.[17b] The

View Article Online
DOI: 10.1039/C5NR01757B
Journal Name

deconvolution of N 1s spectrum indicates that N atoms mainly exist as pyridine-like sp^2-hybridized form (~399.2 eV) and pyrrole-like sp^3-hybridized form (~400.6 eV) (Figure 1f).[8] XRD pattern of E-GQDs shows a broad (002) peak at around 25° (Figure S5b, in SI), consistent with the graphite interlayer spacing of 0.34 nm,[13a] confirming their graphite-like structure. In the Raman spectrum of E-GQDs (Figure S5c, in SI), the D band at ~1360 cm^{-1} shows the specific vibrations at the edges, such as oxides or C=C groups which are only present at the edge,[18a] as well as G band at ~1591 cm^{-1} which originates from the graphitic sheets.[18b] In addition, FT-IR spectroscopy was performed on the EDTA precursor and E-GQDs (Figure S5d, in SI). Compared with EDTA, the product shows significant decrease of C-H stretching vibration at ~2950 cm^{-1} and C–H bending vibration at ~1325 cm^{-1},[19a] as well as the enhancement of absorption band of C=C at ~1655 cm^{-1}, suggesting the formation of sp^2 carbon atoms through the carbonization of EDTA. Moreover, the enhanced band of C-N at ~1360 cm^{-1} proves the nitrogen atoms are doped into the graphene skeleton. Another band of C-O at ~1235 cm^{-1} illustrates the presence of hydroxyl group on graphene sheets.[19b]

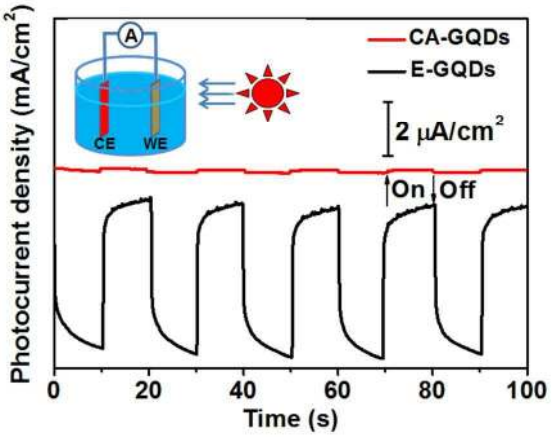

Figure 4. Plot of photocurrent response versus time on the thin films of E-GQDs and CA-GQDs. The bias voltage is 0 V. Inset: The scheme of current measurement system.

The UV-vis absorption spectrum of E-GQDs shows the absorption band at around 340 nm (Figure 3a, dash line). Under the irradiation of a 365 nm lamp, the E-GQDs show very intense blue luminescence (Figure 3a, inset). The photoluminescence (PL) mechanism of GQDs remains somehow controversial in the literature. Generally, it is believed that the PL may be mainly derived from intrinsic state emission and defect state emission.[20a] The former one is induced by the quantum size effect, whereas the latter one depends on the molecule-like states.[20b] The E-GQDs exhibit no obvious PL shift under short excitation wavelength below 365 nm (Figure S6, in SI). As the excitation wavelength increased from 365 to 435 nm, the PL peaks exhibit decreased emission intensity along with remarkable red-shift from 431 to 495 nm (Figure 3a, solid lines). Such excitation-dependent emission indicates the existence of trapping states with different energy levels,[21] which can be attributed to the different surface groups such as C-O, C=O and O=C-OH as revealed by the XPS.

Under the excitation of 365 nm light, the PL quantum yield (QY) is estimated to be 5.1 % (using quinine sulfate as a reference), which is higher than that of undoped GQDs (4.04%)[22] but lower than the carbon dots co-doped with N and S atoms (70%).[12a] In addition, based on the previous study, GQDs have shown strong pH-dependence of the PL intensity, which could decrease when pH is higher than 6 or lower than 4.[22] In contrast, the PL behaviour of our E-GQDs is much less affected by the pH value of solution. The E-GQDs give the maximum emission intensity at pH 3.5, and the intensity maintains above 90% of the maximum value in a wide pH range of 2.5-8.5 (Figure S7, in SI).

The much improved emission properties of E-GQDs as compared to the undoped GQDs, including higher QY and improved pH stability, may result from the N-doping, which enhance the emission of the GQDs by inducing an upward shift in the Fermi level and electrons in the conduction band.[23] The excellent properties of E-GQDs make them more desirable to be used as fluorescent probe for living cell imaging. In this work, the RAW 264.7 (mouse leukemic monocyte macrophage cell line) cells were used to evaluate the cytocompatibility of E-GQDs. The cytotoxicity was examined through testing the cell viability upon exposure to E-GQDs by using the standard cell counting Kit-8 (CCK-8) assay. No apparent reduction in cell viability was found after incubation of the cells with E-GQDs even at its concentration of 140 μg/mL (Figure S8, in SI). Figure 3b shows the fluorescence images of RAW 264.7 cells after being incubated with E-GQDs. The uptake of GQDs can be clearly observed from the strong fluorescence signal in cells. The dark-field (Figure 3c) and the overlay with fluorescence images (Figure 3d) illustrate that most of the fluorescent signal is localized in the cytoplasm, while the fluorescent signal from the nucleus is weak. Furthermore, by comparing the fluorescence and bright-field images with lysosome staining, it is found that most of the intracellular E-GQDs are not in the lysosome (Figure S9, in SI), indicating that the E-GQD cellular uptake may not be related to the endocytic processes. It is believed that the E-GQDs can easily penetrate into the living cells through the non endocytic pathway-like diffusion.[24]

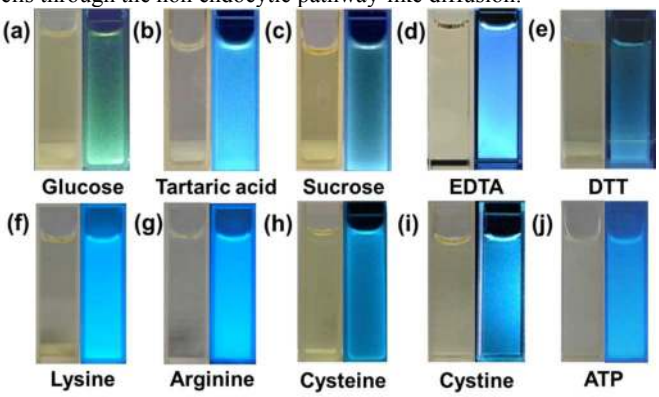

Figure 5. Photographs of various GQDs derived from different precursors in water under daylight (left) and irradiated by 365 nm UV lamp (right).

The unique optical property of E-GQDs offers potential applications in optoelectronics and photo-energy conversion devices.[5,25,26] The thin films of different materials on ITO glass substrates were prepared by electrophoretic deposition and used as working electrodes (WEs). Pt wire and saturated calomel electrode (SCE) were used as counter electrode (CE) and reference electrode (RE), respectively. The WE was irradiated with a 500 W Xe lamp at potential of 0 V (vs. SCE). The undoped GQDs, CA-GQDs, which were prepared using citric acid as precursor and investigated extensively in previous report,[13a] were also studied under the same condition as a reference. SEM and AFM characterization were carried out in order to prove the successful formation of the films. Compact films were observed for both E-GQDs and CA-GQDs (Figure S10a and b, in SI). Figure 4 shows the photocurrent response of the thin films of the two GQDs. The thin film of CA-GQDs exhibits a barely observable photocurrent response with a photocurrent density of only 0.09 $\mu A/cm^2$. In contrast, the film of E-

Journal Name

View Article Online
DOI: 10.1039/C5NR01757B ARTICLE

GQDs gives a photocurrent density of 4.55 μA/cm^2, two orders of magnitude higher compared to that of CA-GQDs, suggesting that the E-GQDs film is much more efficient to produce photocurrent.

To illustrate the generality of this solid-state synthetic method, a variety of small molecules have been tested as precursors for GQD synthesis. Heteroatom-free precursors, such as glucose, tartaric acid and sucrose, were used to produce oxygen containing (O-containing) GQDs. Besides EDTA, some amino acids, including lysine and arginine, can also be used to prepare N-doped GQDs. Moreover, DTT was used to produce S-doped GQDs. GQDs co-doped with N and S atoms were obtained from cysteine and cystine. While GQDs co-doped with N and P atoms were synthesized from ATP. The optimal reaction temperatures for different precursors are different, which are dependent on their decomposition temperature. Similar to that of EDTA, the optimal reaction temperatures for all the precursors were found to be slightly above their decomposition temperatures, as shown on their TGA curves (Figure S11, in SI). Figure 5 shows fluorescence images of various GQDs dispersed in water irradiated by 365 nm UV lamp. All the products show similar blue emission, suggesting that they may have similar molecule-like state.[20] We have also characterized the undoped GQDs derived from glucose (referred to as G-GQDs) for its fluorescence stability and biocompatibility. The UV and PL spectra of G-GQDs are similar to those of E-GQDs (Figure S12, in SI). The G-GQDs with stable PL property that can tolerate a wide pH range of 2.5-8.5 (Figure S13, in SI). Moreover, the cytotoxicity of G-GQDs indicates that the cell viability is maintained at high concentration of G-GQDs at 100 μg/mL (Figure S14, in SI).

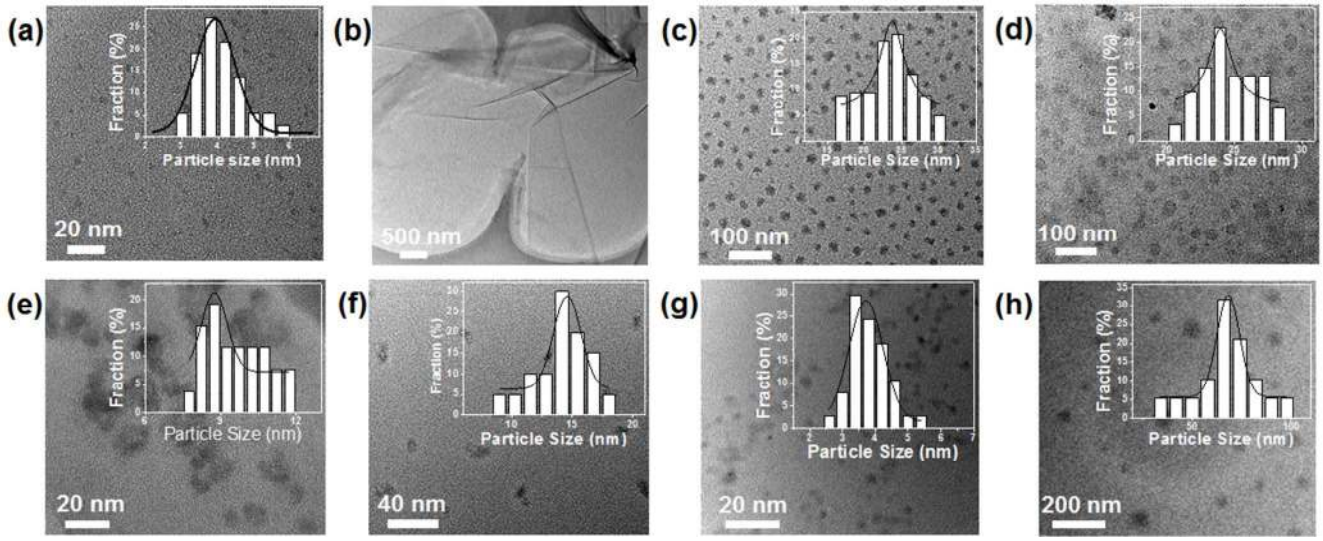

Figure 6. (a) TEM image of GQDs derived from (a) arginine. Inset: size distribution with Gaussian fitting curve. The average size is 4.5 ± 1.5 nm. (b) TEM image of large flakes obtained with arginine as precursor at longer reaction time. TEM image of GQDs derived from (c) lysine (23.5 ± 6.6 nm), (d) tartaric acid (24.5 ± 3.8 nm), (e) sucrose (9.8 ± 2.0 nm), (f) cysteine (13.5 ± 4.6 nm), (g) cystine (3.8 ± 1.6 nm) and (h) DTT (66 ± 32 nm). Insets show the size distributions.

Successful heteroatom doping were confirmed by the XPS spectra of different samples. The XPS spectrum of the GQD from lysine has strong N 1s peak. The deconvolution of the N 1s spectrum indicates that the doped N atoms mainly exist as quaternary N with small amount of pyrrolic N (Figure S15, in SI). The strong S 2p peak from the sample synthesized from DTT indicates significant amount of doped S atom. The deconvolution of the S 2p spectrum shows the evidence for presence of C-S, sulfoxide and other oxidized forms (Figure S16, in SI). The sample synthesized from cysteine exhibits both N and S signals suggesting co-doping of the two heteroatoms (Figure S17, in SI). The XPS spectra of GQDs synthesized from ATP indicates strong N 1s and P 2p peaks confirming co-doping of N and P. Careful deconvolution of the N 1s and P 2p peaks reveals that N atoms mainly exist as pyridine-like sp^2-hybridized form and pyrrole-like sp^3-hybridized form, while the P atoms are mainly bonded to C atoms (Figure S18, in SI). It is worth noting that the GQD co-doped with N and P atoms has not been synthesized before.

The dopant concentrations in the products from different precursors are compared in Table S3. It has been proven that N doping or amino-group functionalization significantly change the optical properties of GQDs.[27] Herein, the products from EDTA, lysine, cysteine and ATP possess N/C ratio of 32.4%, 24.1%, 20.3% and 46.8%, respectively. It has been reported that appropriate doping of N gave rise to a more efficient PL radiative emission, but, excessive N dopants could lead to PL quenching.[28] The unstable surface defects, which lead to reduced radiative recombination, confine the QY of GQDs.[29] Similar phenomenon has been observed in our experiment. The optimal N/C atomic ratio is found to be around 24.1% (Figure S19), and the product from lysine shows the highest QY. The QY of all the products based on the different precursors are compared in Figure S20, suggesting a complicated influence of atomic composition to their PL properties.

All the GQDs exhibit significant photocurrent response but the intensities of the photocurrent are different (Figure S21). The E-GQD gave the highest photocurrent but the products based on tartaric acid, lysine and ATP do not show appreciable photocurrent. Previous report has drawn the conclusion that N-doped graphene and N-doped graphene nanoribbons exhibit n-type conductivity due to nitrogen present in the π-conjugated system, and the amount of N atoms in N-doped GQDs endows the substantial improvement of photocurrent response.[30] Therefore, the high photo-response from E-GQD may due to the fact that it has a high N atom concentration (14.3%) (Table S3). However, this mechanism may not apply for products from sucrose, DTT and glucose since they have no N-dopant. For these N-free GQDs, photon absorption associated with the molecule-like state and spatial separation of photogenerated electrons and holes.[31] Other factors that promote the photocurrent response may include effects of electron-rich heteroatoms like sulfur (cases of cysteine and DTT), which can provide more electrons to generate photocurrents. However, the decisive mechanism could be complicated and the photocurrent response properties are affected by a combination of a series of different factors.

The TEM analysis showed the uniform particle sizes at optimal conditions obtained from the precursors including arginine (Figure

View Article Online
DOI: 10.1039/C5NR01757B Journal Name

6a), lysine, tartaric acid, sucrose, cysteine, cystine and DTT (Figure 6c-h). Similarly, the graphene sheet with micron size can be formed if the reaction for arginine reaches 10 min or more (Figure 6b). The GQDs derived from glucose and ATP also have uniform particle sizes (Figure 7a and c). The HRTEM images show clearly visible lattice fringes (Figure 7b and d), indicating highly crystalline structure. However, we did not obtain clear lattice fringes for the other particles prepared from arginine, lysine, tartaric acid, sucrose, cysteine, cystine and DTT, so they might be better to be described as carbon dots. The unperceived lattice fringe can be attributed to the lattice structure disordered by introducing of heteroatom.

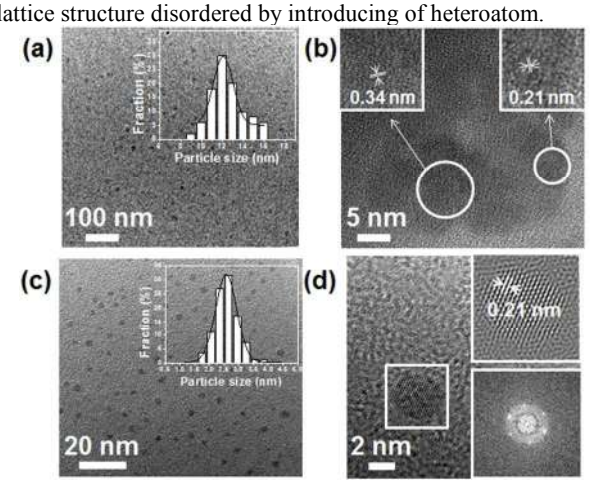

Figure 7. (a) TEM image of GQD (a) TEM image of G-GQDs. Inset: size distribution with Gaussian fitting curve. The average size is 12.1 ± 3.5 nm. (b) HRTEM image of G-GQDs, showing lattice fringes of 0.34 nm and 0.21 nm. (c) TEM image of GQDs derived from ATP. Inset: Size distribution with Gaussian fitting curve. The average size is 2.8 ± 1.0 nm. (d) HRTEM image of GQDs derived from ATP. Insets: (top) FFT-filtered HRTEM image, (bottom) the corresponding FFT of the HRTEM image highlighted in the white square in (d).

Conclusions

In summary, we have developed a facile general method to synthesize various chemically doped GQDs, which is based on solid reaction of a variety of simple organic precursors. The produced GQDs exhibit high fluorescence, good pH stability and low cyto-toxicity, making them suitable for bio-labelling and optoelectronic applications. As demonstrated herein, this method can be extended to a wider range of precursors, opening a new avenue for the rational design and low cost production of different types of heteroatom doped GQDs. Further investigation including applications of the various doped GQDs in biology and optoelectronics are underway.

Acknowledgements

This work is supported by National Basic Research Program of China (973 Program) No.2012CB933102, National Natural Science Foundation of China (NSFC. 21233001, 21190034, 21073079), Specialized Research Fund for the Doctoral Program of Higher Education (SRFDP. 20110211130001), the Fundamental Research Funds for the Central Universities and 111 Project.

Notes and references

[a]State Key Laboratory of Applied Organic Chemistry (SKLAOC), Key Laboratory of Special Function Materials and Structure Design (MOE), College of Chemistry and Chemical Engineering Lanzhou University, Lanzhou, 730000, P. R. China, E-mail: Haoli.zhang@lzu.edu.cn.
[b]School of Materials Science and Engineering, Nanyang Technological University, 50 Nanyang Avenue, Singapore 639798, Singapore. E-mail: hzhang@ntu.edu.sg;
[c]Singapore Institute of Manufacturing Technology, 71 Nanyang Drive, Singapore 638075, Singapore.
[d]Advanced Membranes and Porous Materials Center, Physical Sciences and Engineering Division, King Abdullah University of Science and Technology, Thuwal 23955-6900, Saudi Arabia
[e]Key Laboratory of Magnetism and Magnetic Materials of Ministry of Education, School of Physical Science and Technology, Lanzhou University, Lanzhou 730000, China
Electronic Supplementary Information (ESI) available: [details of any supplementary information available should be included here]. See DOI: 10.1039/c000000x/

1 V. Gupta, N. Chaudhary, R. Srivastava, G. D. Sharma, R. Bhardwaj and S. Chand, *J. Am. Chem. Soc.,* 2011, **133**, 9960-9963.
2 X. Sun, Z. Liu, K. Welsher, J. T. Robinson, A. Goodwin, S. Zaric and H. Dai, *Nano Res.,* 2008, **1**, 203-212.
3 Z. Liu, J. T. Robinson, X. Sun and H. Dai, *J. Am. Chem. Soc.,* 2008, **130**, 10876-10877.
4 (a) L. A. Ponomarenko, F. Schedin, M. I. Katsnelson, R. Yang, E. W. Hill, K. S. Novoselov and A. K. Geim, *Science,* 2008, **320**, 356-358; (b) Y. Li, Y. Hu, Y. Zhao, G. Shi, L. Deng, Y. Hou and L. Qu, *Adv. Mater.,* 2011, **23**, 776-780.
5 J. Shen, Y. Zhu, X. Yang, J. Zong, J. Zhang and C. Li, *New J. Chem.,* 2012, **36**, 97-101.
6 R. Ye, C. Xiang, J. Lin, Z. Peng, K. Huang, Z. Yan, N. P. Cook, E. L. Samuel, C. C. Hwang, G. Ruan, G. Ceriotti, A. R. Raji, A. A. Marti and J. M. Tour, *Nat.Commun.,* 2013, **4**, 2943.
7 (a) Y. Zhang, K. Zhou, K. Xie, J. Zeng, H.-L. Zhang and Y. Peng, *Nanotechnology,* 2010, **21**, 065201; (b) Y.-C. Zhou, H.-L. Zhang and W.-Q. Deng, *Nanotechnology,* 2013, **24**, 225705; (c) M. Latorre-Sanchez, A. Primo and H. Garcia, *Angew. Chem. Int. Ed.,* 2013**, 52**, 11813-11836; (d) S. U. Lee, R. V. Belosludov, H. Mizuseki and Y. Kawazoe, *Small,* 2009, **5**, 1769-1775.
8 Y. Li, Y. Zhao, H. Cheng, Y. Hu, G. Shi, L. Dai and L. Qu, *J. Am. Chem. Soc.,* 2012, **134**, 15-18.
9 (a) X. Li, S. P. Lau, L. Tang, R. Ji and P. Yang, *J. Mater. Chem. C,* 2013, **1**, 7308-7313; (b) Z. Wu, M. Gao, T. Wang, X. Wan, L. Zheng and C. Huang, *Nanoscale,* 2014, **6**, 3868-3874.
10 (a) Q. Liu, B. Guo, Z. Rao, B. Zhang and J. R. Gong, *Nano Lett.,* 2013, **13**, 2436–2441; (b) Z. Qian, J. Ma, X. Shan, H, Shan, L. Shao and J. Chen, *Chem. Eur. J.*, 2014, **20**, 2254-2263; (c) Z. Qian, X. Shan, L. Chai, J. Ma, J. Chen, and H. Feng, *ACS Appl. Mater. Interfaces,* 2014, **6**, 6797-6805; X. Shan, L. Chai, J., Z. Qian, J. Chen and H. Feng, *Analyst*, 2014, **139**, 2322-2325; (d) J. Zhou, X. Shan, J. Ma, Y. Gu, Z. Qian, J. Chen and H. Feng, *RSC Adv.*, 2014, **4**, 5465-5468.
11 (a) Q. Li, S. Zhang, L. Dai and L.-s. Li, *J. Am. Chem. Soc*., 2012, **134**, 18932-18935; (b) X. Chen, Q. Jin, L. Wu, C.H.

View Article Online
DOI: 10.1039/C5NR01757B ARTICLE

Tung and X. Tang, *Angew. Chem. Int. Ed*., 2014, **53**, 12542-12547.

12 (a) Y. Dong, H. Pang, H.Yang, C. Guo, J. Shao, Y. Chi, C. Li and T. Yu, *Angew. Chem. Int. Ed.,* 2013, **52**, 7800-7804; (b) S. Zhu, Q. Meng, L. Wang, J. Zhang, Y. Song, H. Jin, K. Zhang, H. Sun, H. Wang and B. Yang, *Angew. Chem. Int. Ed.,* 2013, **52**, 3953-3957.

13 (a) Y. Dong, J. Shao, C. Chen, H. Li, R. Wang, Y. Chi, X. Lin and G. Chen, *Carbon,* 2012, **50**, 4738-4743; (b) D. Pan, J. Zhang, Z. Li, C. Wu, X. Yan and M. Wu, *Chem. Commun.,* 2010, **46**, 3681-3683.

14 R. j. M. A. E. Martell, A. R. Fried, J. S. Wilson, and D. T. Macmillan, *Can. J. Chem.,* 1975, **53**, 3471-3476.

15 J. Zhang, X. Chen, K. Takanabe, K. Maeda, K. Domen, J. D. Epping, S. Fu, M. Antonietti and X. Wang, *Angew. Chem. Int. Ed*., 2010, **49**, 441-444.

16 (a) N. Y. Jin-Phillipp and M. Rühle, *Phys. Rev. B.,* 2004, **70**, 245421; (b) M. Endo, K. Takeuchi, T. Hiraoka, T. Furuta, T. Kasai, X. Sun, C. H. Kiang and M. S. Dresselhaus, *J. Phys. Chem. Solids,* 1997, **58**, 1707–1712.

17 (a) V. Datsyuka, M. Kalyva, K. Papagelis, J. Parthenios, D. Tasis, A. Siokou, I. Kallitsis and C. Galiotis, *Carbon,* 2008, **46**, 833-840; (b) P. Srinivasu, A. Islam, S. P. Singh, L. Han, M. L. Kantam and S. K. Bhargava, *J. Mater. Chem.,* 2012, **22**, 20866-20869.

18 (a) Y. Wang, D. C. Alsmeyer and R. L. McCreery, *Chem. Mater.,* 1990, **2**, 557-563; (b) W. B. Choi, D. S. Chung, J. H. Kang, H. Y. Kim, Y. W. Jin, I. T. Han, Y. H. Lee, J. E. Jung, N. S. Lee, G. S. Park and J. M. Kim, *Appl. Phys. Lett.,* 1999, **75**, 3129.

19 (a) Y. Yang, J. Cui, M. Zheng, C. Hu, S. Tan, Y. Xiao, Q. Yang and Y. Liu, *Chem. Commun.,* 2012, **48**, 380-382; (b) S. Stankovich, R. D. Piner, S. T. Nguyen and R. S. Ruoff, *Carbon,* 2006, **44**, 3342-3347.

20 (a) H. Sun, L. Wu, W. Wei and X. Qu, *Mater. Today*, 2013, **16**, 433-442; (b) L. Wang, S.-J. Zhu, H.-Y. Wang, S.-N. Qu, Y.-L. Zhang, J.-H. Zhang, Q.-D. Chen, H.-L. Xu, W. Han, B. Yang and H.-B. Sun, *ACS Nano*, 2014, **8**, 2541-2547.

21 (a) X. Li, S. Zhang, S. A. Kulinich, Y. Liu and H. Zeng, *Sci. Rep.,* 2014, **4**, 4976; (b) L. Wang, S.-J. Zhu, H.-Y. Wang, Y.-F. Wang, Y.-W. Hao, J.-H. Zhang, Q.-D. Chen, Y.-L. Zhang, W. Han, B. Yang and H.-B. Sun, *Adv. Optical Mater.*, 2013, **1**, 264–271; (c) V. Strauss, J. T. Margraf, C. Dolle, B. Butz, T. J. Nacken, J. Walter, W. Bauer, W. Peukert, E. Spiecker, T. Clark and D. M. Guldi, *J. Am. Chem. Soc*., 2014, **136**, 17308−17316.

22 Y. Dong, C. Chen, X. Zheng, L. Gao, Z. Cui, H. Yang, C. Guo, Y. Chi and C. Li, *J. Mater. Chem.,* 2012, **22**, 8764-8766.

23 (a) Y. Wang and A. Hu, *J. Mater. Chem. C*, 2014, **2**, 6921–6939; (b) P. Ayala, R. Arenal, A. Loiseau, A. Rubio and T. Pichler, *Rev. Mod. Phys.*, 2010, **82**, 1843.

24 N. Li, X. Liang, L. Wang, Z. Li, P. Li, Y. Zhu and J. Song, *J. Nanopart. Res.,* 2012, **14**, 1177-1186.

25 X. Zhang, Y. Zhang, Y. Wang, S. Kalytchuk, S. V. Kershaw, Y. Wang, P. Wang, T. Zhang, Y. Zhao, H. Zhang, T. Cui, Y. Wang, J. Zhao, W. W. Yu and A. L. Rogach, *ACS Nano*, 2013, **7**, 11234–11241.

26 S. H. Jin, D. H. Kim, G. H. Jun, S. H. Hong and S. Jeon, *ACS Nano,* 2013, **7**, 1239-1245.

27 (a) D. Wei, Y. Liu, Y. Wang, H. Zhang, L. Huang and G. Yu, *Nano Lett*., 2009, **9**, 1752-1758; (b) C. Wang, Y. Zhou, L. He, T. Ng, G. Hong, Q. Wu, F. Gao, C. Lee and W. Zhang, *Nanoscale,* 2013, **5**, 600-605; (c) H. Tetsuka, R. Asahi, A. Nagoya, K. Okamoto, I. Tajima, R. Ohta and A. Okamoto, *Adv. Mater.*, 2012, **24**, 5333-5338.

28 Y. Dai, H. Long, X. Wang, Y.Wang, Q.Gu, W.Jiang, Y. Wang, C. Li, T. H. Zeng, Y. Sun and J. Zeng, *Part. Part. Syst. Charact*., 2014, **31**, 597–604.

29 S. Y. Lim, W. Shen and Z. Gao, *Chem. Soc. Rev.*, 2015, **44**, 362-381.

30 X. Wang, D. Ling, Y. Wang, H. Long, Y. Sun, Y. Shi, Y. Chen, Y. Jing, Y. Sun and Y. Dai, *J. Mater. Res.*, 2014, **29**, 1408-1416.

31 S.-H. Cheng, T.-M. Weng, M.-L. Lu, W.-C. Tan, J.-Y. Chen and Y.-F. Chen, *Sci. Rep.*, 2013, **3**, 2694.